Nuclear Instruments and Methods in Physics Research A 1093 (2027) 172023

Contents lists available at ScienceDirect

Nuclear Inst. and Methods in Physics Research, A

journal homepage: www.elsevier.com/locate/nima

Full Length Article

nuSCOPE: A monitored and tagged neutrino beam☆

A. Falcone [1,*], F. Acerbi [2,3], C. Andreopoulos [4], I. Angelis [5], A. Baratto Roldan [6], L. Bomben [1,7], M. Bonesini [1], F. Bramati [1,8], A. Branca [1,8], C. Brizzolari [1,8], G. Brunetti [8], M. Buizza Avanzini [9], S. Capelli [1,7], M. Capitani [29,6], S. Carturan [10,11], M.G. Catanesi [12], S. Cecchini [13], N. Charitonidis [6], F. Cindolo [13], J. Cogan [14], G. Cogo [10], G. Collazuol [10,15], D. D'Ago [15], F. Dal Corso [15], G. De Rosa [16,17], S. Dolan [6], M. Feltre [10,15], A. Gola [2], D. Guffanti [1,8], L. Halić [18], F. Iacob [10,15], M.A. Jebramcik [6], C. Jollet [19], A. Kallitsopoulou [20], B. Kliček [18], A. Lai [21], Ch. Lampoudis [5], F. Lanni [6], M. Laveder [10,15], P. Legou [20], S. Levorato [15], A. Longhin [10,15], L. Ludovici [22], L. Magaletti [12,23], G. Mandrioli [13], A. Margotti [13], V. Mascagna [25,26], M. Mattiazzi [10,15], N. Mauri [13,24], J. McElwee [19], L. Meazza [1,8], A. Meregaglia [19], M. Mezzetto [15], L. Munteanu [6], A. Paoloni [27], M. Pari [6], T. Papaevangelou [20], E.G. Parozzi [1,6,8], L. Pasqualini [13,24], G. Paternoster [2], L. Patrizii [13], M. Perrin-Terrin [14], L. Petit [14,28], M. Pozzato [13], M. Prest [1,7], F. Pupilli [15], E. Radicioni [12], F. Resnati [6], A.C. Ruggeri [16,17], A. Roueff [28], G. Saibene [1,7], D. Sampsonidis [5], A. Scanu [1,8], C. Scian [10,15], G. Sirri [13], R. Speziali [1,8], M. Stipčević [18], M. Tenti [13], F. Terranova [1,8], M. Torti [1,8], S.E. Tzamarias [5], E. Vallazza [1], C. Vallée [28], L. Votano [27]

[1] INFN Sezione di Milano-Bicocca, Piazza della Scienza 3 20133 Milano, Italy
[2] Fondazione Bruno Kessler (FBK), Via Sommarive 18 38123 Povo (TN), Italy
[3] INFN-TIFPA, Universitá di Trento, Via Sommarive 14 38123 Povo (TN), Italy
[4] University of Liverpool, Department of Physics, Liverpool L69 7ZE, UK
[5] Aristotle University of Thessaloniki, Thessaloniki 541 24, Greece
[6] CERN, Esplanade des particules, 1211 Geneve 23, Switzerland
[7] Universitá degli Studi dell' Insubria, Via Valleggio 11 22100 Como, Italy
[8] Universitá di Milano-Bicocca, Piazza della Scienza 3 20133 Milano, Italy
[9] Ecole Polytechnique, IN2P3-CNRS, Laboratoire Leprince-Ringuet, Palaiseau, France
[10] Universiá di Padova, via Marzolo 8 35131 Padova, Italy
[11] INFN, Laboratori Nazionali di Legnaro, Viale dell'Universitá 2 35020 Legnaro (PD), Italy
[12] INFN Sezione di Bari, Via Giovanni Amendola 173 70126 Bari, Italy
[13] INFN Sezione di Bologna, viale Berti-Pichat 6-2 40127 Bologna, Italy
[14] Aix Marseille Univ, CNRS/IN2P3, CPPM, Marseille, France
[15] INFN Sezione di Padova, via Marzolo 8 35131 Padova, Italy
[16] INFN Sezione di Napoli, Strada Comunale Cinthia 80126 Napoli, Italy
[17] Universitá "Federico II" di Napoli, Corso Umberto I 40 80138 Napoli, Italy
[18] Center of Excellence for Advanced Materials and Sensing Devices, Ruder Boskovic Institute, HR-10000, Zagreb, Croatia
[19] LP2I Bordeaux, Université de Bordeaux, CNRS/IN2P3, 33175 Gradignan, France
[20] CEA, Centre de Saclay, Irfu/SPP, F-91191 Gif-sur-Yvette, France
[21] INFN Sezione di Cagliari, Cagliari, Italy
[22] INFN Sezione di Roma 1, Piazzale A. Moro 2, 00185 Rome, Italy
[23] Universitá di Bari, Via Giovanni Amendola 173 70126 Bari, Italy
[24] Universitá degli Studi di Bologna, viale Berti-Pichat 6 40127 Bologna, Italy
[25] DII, Universitá degli Studi di Brescia, via Branze 38, Brescia, Italy
[26] INFN Sezione di Pavia, via Bassi 6, 27100 Pavia, Italy
[27] INFN, Laboratori Nazionali di Frascati, via Fermi 40 00044 Frascati (Rome), Italy
[28] Université de Toulon, Aix Marseille Univ, CNRS, IM2NP, Toulon, France

☆ This article is part of a Special issue entitled: 'TIPP 2026' published in Nuclear Inst. and Methods in Physics Research, A.

* Corresponding author.
E-mail address: andrea.falcone@mib.infn.it (A. Falcone).

https://doi.org/10.1016/j.nima.2026.172023
Received 14 May 2026; Received in revised form 22 August 2026; Accepted 26 August 2026
Available online 2 September 2026
0168-9002/© 2026 The Authors. Published by Elsevier B.V. This is an open access article under the CC BY license (http://creativecommons.org/licenses/by/4.0/).

[29] Department of Physics, University of Ioannina, Ioannina 451 10, Greece

ARTICLE INFO

Keywords:
Neutrino beam
Monitored beam
Tagged beam

ABSTRACT

The poor knowledge of neutrino cross sections at the GeV scale is projected to be responsible for some of the leading sources of uncertainty in next-generation oscillation experiments. The nuSCOPE experiment is based on the ideas and R&D from ENUBET and NuTAG, to build a high-precision, short-baseline neutrino experiment at CERN that employs neutrino monitoring and tagging. It allows for an exceptionally well controlled muon and electron neutrino flux, with the extraordinary capacity to reconstruct neutrino energy on an event-by-event basis. This opens up the possibility for a wealth of measurements usually reserved only for electron-scattering experiments. In this paper we describe the beamline instrumentation, demonstrating the experiment unique ability to directly measure aspects of neutrino interaction physics responsible for dominant sources of systematic uncertainty for the upcoming DUNE and Hyper-K experiments.

1. Introduction

Beam neutrino physics is upon entering in its precision era with the starting of the DUNE and Hyper-Kamiokande experiments. They will have unprecedented beam power and detector mass, pushing statistical uncertainties far below the systematic budget. Cross-section uncertainties will become the dominant factor limiting the physics reach of these experiments, and the construction of high-precision cross-section experiments offers the most robust and cost-effective pathway to solve the problem. Significant theoretical challenges limit the evaluation of neutrino cross-sections in the 1–5 GeV energy range [1] and state-of-the-art generators cannot achieve better than 30% agreement with experimental data.

Moreover, contrary to what happen with charged lepton beams, where the incoming particles can be determined in flux, flavor (e, μ) and energy with a precision well below a few percent, enabling a detailed study of lepton scattering processes, for neutrinos the flux is typically known with a precision of about 10%, and the energy can only be inferred indirectly from the four-momentum of the final-state particles. Consequently, despite considerable progress in neutrino scattering measurements achieved through the near detectors of T2K and NOνA, as well as dedicated cross-section experiments such as SciBooNE, MINERvA, LArIAT, and MicroBooNE [2], the precision of neutrino cross section measurements remains insufficient for the demands of high-precision neutrino oscillation physics. A new generation of high-precision neutrino beams can be capable of addressing these limitations. The ENUBET Collaboration had the aim to develop a monitored narrow-band neutrino beam, whose neutrino flux is known with an unprecedented precision of 1%, to enable ν_μ and ν_e cross-section measurements [3]. The collaboration successfully designed a beamline capable of producing a moderate-intensity neutrino flux from π and K decays, without relying on magnetic horns [4]. In this way, primary protons could be delivered to the target in long extractions, lasting several seconds, rather than the typical 10 μs to 1 ms bursts. The longer extractions reduce the instantaneous rate of charged leptons by several orders of magnitude, and enable a precise monitoring of neutrino fluxes with the direct detection of the large angle muons and positrons from kaon decays in the decay tunnel walls and of forward muons from pion decays in an instrumented hadron dump. The several seconds bunch unlocks the possibility of a tagged neutrino beam, proposed by the NuTag Collaboration [5]. It would constitute a groundbreaking advancement in experimental physics, enabling the direct measurement of neutrino energy on an event-by-event basis using the two-body kinematics of the parent meson decay. The ENUBET beamline can be equipped with fast (<100 ps resolution), radiation-hard silicon trackers, to track both the parent meson and its daughter charged leptons. The advanced lepton tracking offers a direct and precise flux measurement and spectral characterization, without relying on MC simulation of the beamline. Moreover, if the downstream neutrino detector possesses sufficient time resolution (<1 ns), each observed neutrino can be uniquely correlated with its parent meson and associated charged lepton, accomplishing a "tagged neutrino beam". In 2023, the convergence of the ENUBET and NuTag led to the international collaboration nuSCOPE — neutrino SPS COmplex for Precision Experiments [6].

Table 1
Beamline parameters and specifications of the newly optimized nuSCOPE beamline at SPS energies. Meson yields and rates refer to the location at the beginning of the decay tunnel. The total proton requirement targets a 1% statistical uncertainty on the inclusive ν_e cross-section. The annual proton intensity assumes a spill duration of 9.6 s.

Parameter	Value
Primary p momentum	400 GeV/c
Beamline meson momentum	peaked at 8.5 GeV/c
p-beam spill duration	slow (4.8 s to 9.6 s)
Spill intensity	1×10^{13} p/spill
Event rate	1–2 THz
Instantaneous power on target	170–340 W
(K^+, π^+)	(1.3, 19×10^{-3}) yield per p
(K^+, π^+) rate	max. (2.7, 40) GHz
Annual p intensity	$2.1–3.2 \times 10^{18}$ p/year
Total proton requirement	1.4×10^{19} p

The proposed beamline is detailed in Section 2. The flux of outgoing neutrinos originating from kaon decays and reaching the detectors can be monitored by the instrumentation in the tunnel walls, as discussed in Section 3. The ν_μ flux from pion decays is primarily monitored by the instrumented hadron dump, as described in Section 4. The silicon planes, to tag neutrinos at the single-particle level by tracking their parent mesons and daughter muons, are described in Section 5. The downstream neutrino detector characteristics are summarized in Section 6. Section 7 briefly describe the technique that enables a sub-percent precision measurement of the neutrino flux using lepton monitoring and tracking, and the two methods by which nuSCOPE can measure the neutrino energy without relying on neutrino interactions: the Narrow Band Off-Axis technique which achieves a precision of approximately O(10)%, and the tagging method, which can reach the ultimate precision of ∼1%. Example of cross-section measurements made possible by such a facility are finally detailed in Section 8.

2. Beamline design

The nuSCOPE beamline, shown in Fig. 1, aims at producing kaons and pions at 8.5 GeV/c with a ∼10% momentum bite. It is optimized to produce an ideally monochromatic meson beam that remains parallel throughout the 40 m-long decay tunnel. The preliminary beamline specifications are listed in Table 1. The total proton requirement targets a 1% statistical uncertainty on the inclusive ν_e cross-section.

The proton beam impinge on a graphite target to produce the mesons. The three initial quadrupoles downstream of the target provide the necessary transverse phase advance to allow as many particles as possible to pass through the beamline momentum selection. It is

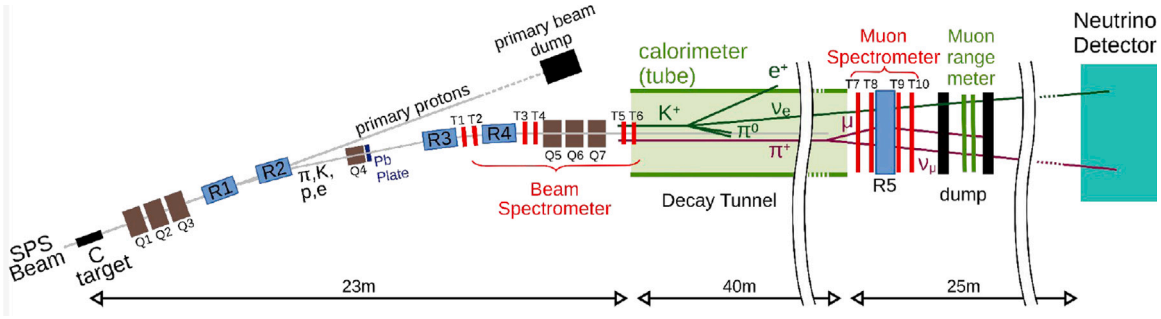


Fig. 1. Layout of the experimental setup of the nuSCOPE beamline. The beamline (not to scale) combines both the ENUBET (in green) and the NuTag (in red) beam instrumentation. The first part of the beamline contains the beamline magnets (blue: rectangular bending magnets; brown: quadrupole magnets).

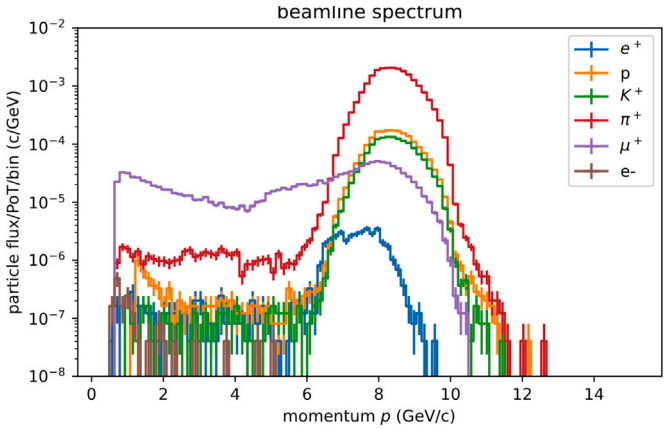


Fig. 2. nuSCOPE beamline spectrum after the optimization process.

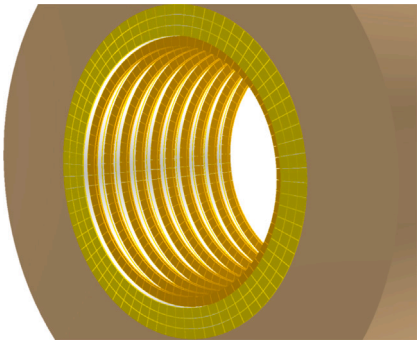


Fig. 3. Instrumented decay tunnel scheme. The three layers of modules of the calorimeter (light green) constitute the inner wall of the tunnel. The rings of the scintillator tiles of the photon veto (yellow) are located just below the modules. The optical fibers (not shown) bring the light to the outer part of the tunnel in the radial direction. They cross the neutron shielding (light brown) where the SiPMs (not shown) are positioned.

performed by bending magnets with small vertical gaps that deflect the secondary beam by 18°. This section removes particles with momenta outside the desired momentum range, typically a ±10% relative momentum range around the chosen one. The final quadrupole triplet produces the parallel beam in the decay tunnel.

The starting point of the present beamline design was an update of the ENUBET beamline baseline design [4]. The production target and the beamline optics were matched to each other very carefully and both optimized in a self-consistent manner. Since the pixel detectors for particle tagging present a maximum read-out rate of O(100 MHz/mm^2) (see Section 5), the optimization is aimed at O(10 MHz/mm^2) to suppress pile-up. To mitigate the large number of positrons that are produced in the graphite target, a thin Pb plate is inserted into the beamline right after the Q4 quadrupole to degrade their energy outside the beamline acceptance. The spectrum of the particles transmitted by the optimized beamline at the entrance of the decay tunnel is shown in Fig. 2 with the beamline momentum set to p = 8.5 GeV/c.

Another critical parameter for the beamline is the particle rate at the pixel detectors that are used for the momentum reconstruction at the R4 bending magnet (see Fig. 1). However, with the spill intensity of 1 × 10^{13} PoT within 9.6 s, the particle flux is in the range of 10–40MHz/mm^2, that is fully acceptable.

3. Neutrino monitoring in the tunnel wall

The decay tunnel walls will be instrumented with a coarse sampling calorimeter, a cost-effective solution for the full coverage of its 40 m length, and with a photon veto ("t$_0$ layer"), as sketched in Fig. 3. The calorimeter will monitor the ν_e flux and the high-energy component of the ν_μ flux, measuring the charged leptons emitted at large angles from kaon decays.

The calorimeter is employed to achieve e+/π+/μ+ separation. It is segmented in the longitudinal, azimuthal and radial directions; the basic unit, called Lateral Compact Module (LCM), is made of five slabs of iron interleaved with tiles of plastic scintillator. The transverse size of the iron and scintillator tiles is 3 × 3 cm^2 and the thickness is 1.5 and 0.7 cm, respectively, for a total thickness of a LCM of 11 cm, corresponding to 4.3 X$_0$. The LCMs are arranged in three radial layers, with every module covering an azimuthal angle of 31 mrad for a total of 200 LCMs per layer at a fixed longitudinal position along the tunnel. The t$_0$ layer is used to distinguish e.m. showers due to γs from the ones due to positrons and to provide the absolute time of each charged particle impinging on the tunnel walls. It is composed by rings of plastic scintillator tiles, placed in the innermost part of the tunnel, in correspondence of the first two tiles of each LCM. The scintillation light produced by both calorimeter and t$_0$ layer modules is routed by a couple of WLS fibers, placed on the front face of each scintillator tile, towards SiPMs. They are placed above a 30 cm thick borated polyethylene shielding that protects against neutron radiation damage of the sensors. The 10 fibers of each LCM are read out together, while each t$_0$ layer tile is read out individually; the corresponding SIPMs are connected to digitizers that sample the resulting waveforms [7]. A large-scale prototype (1.65 m length, 90° azimuthal coverage) of the instrumented decay tunnel was constructed and exposed to mixed charged-particle beams in the T9 secondary line of the CERN-PS for validation in 2022–24 [8]. Collected data confirm the viability of the proposed solution, already tested with smaller prototypes [9], in terms of energy resolution (~17% at 1 GeV) and charged particle identification for neutrino monitoring, and are used to fine-tune the detector simulation.

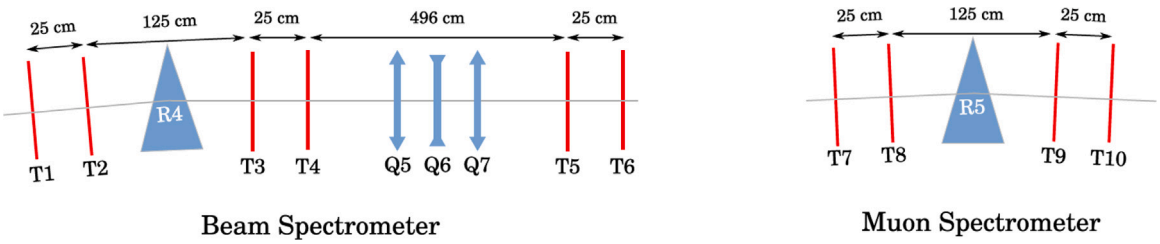


Fig. 4. Layout of the beam (left) and muon (right) spectrometers.

A full Geant4 simulation of the 40 m long tunnel has been developed. It tracks all the particles at the tunnel entrance derived from the output of the beamline simulation, and records in each detector module the energy deposition from the particles impinging the tunnel walls. This framework has been used to develop and assess the performance of the charged lepton identification algorithms in the decay tunnel [7].

4. Instrumented hadron dump

The beam π^+ decays produce muons in pair with neutrinos that are almost collinear with the axis of the tunnel. This low-energy component of the ν_μ flux cannot be monitored through the instrumented tunnel, since it is outside the geometric acceptance of the calorimeter. Only detectors installed downstream of the hadron dump allow the measurement of forward muons exiting the tunnel; the narrow-band beam and the slow proton extraction time of the nuSCOPE facility are useful for identifying these muons and achieving precise control of the neutrino flux. We plan to install different detector layers at increasing depth, interleaved by absorbing material, so that the spatial distribution and energy of the muons can be measured by range out. The detector layers will be installed after the hadron dump, which is dimensioned to absorb the entire hadronic component of the beam from the decay tunnel. A preliminary configuration of the muon detection system has already been studied. The hadron dump is a 2 m long iron slab. The first muon station is placed after the dump, followed by another 2 m iron absorber. Seven additional muon stations follow the first station, interleaved with 0.5 m wide iron absorbers. The total number of muon stations was chosen in such a way that no muons are left after the last station. The GEANT4 simulation of the muon system shows that the muon rate at the first muon station, where the highest rates are observed, has a maximum value of 2.5 MHz/cm^2, corresponding to the bulk of the muon beam. The evaluated rate is within the specifications of a high-granularity fast tracking detector such as the MicroMegas (MM) or picosecond MM [10]. Tests with prototype detectors will be carried out to evaluate the final detector technology.

5. Spectrometers for neutrino tagging

In order to kinematically reconstruct the neutrinos produced in $K^+ \to \mu^+\nu_\mu$ and $\pi^+ \to \mu^+\nu_\mu$ decays, the beamline is instrumented with two spectrometers measuring momentum, direction, time, and position of charged beam particles and their decay products. These beam and muon spectrometers are positioned upstream and downstream of the decay tunnel respectively. Each spectrometer consists of a dipole magnet installed between two pairs of silicon pixel tracking planes. To minimize the length of the region upstream of the decay tunnel, where K^+ and π^+ decays cannot be reconstructed, the beam spectrometer exploits the last dipole magnet (R4) of the front-end beamline. Since the field map of the quadrupole triplet (Q5-7) downstream of R4 may vary, the beam spectrometer includes two additional tracking planes (T5-6), positioned at the decay tunnel entrance, to precisely measure the beam particle direction. The spectrometer reference layouts are shown in Fig. 4.

To allow for a correct association of the neutrino interaction with its parent decay, the spectrometers momentum and angular resolutions are essential. With a minor adjustment of the tracking plane spacing, the contribution of the tracking plane spatial resolution to the spectrometer momentum and angular resolutions can be made smaller than that from multiple Coulomb scattering. A material budget per plane of approximately 1% of a radiation length is sufficient to meet the requirements of the tagging technique. The tracking plane sizes were chosen to provide the largest ratio between the number of reconstructed decays and the total tracking plane surface.

Tracking planes for the muon spectrometer are notably larger than for the beam spectrometer, due to beam divergence and the muon emission angle. The tracking plane surfaces are 12×10 cm^2 in T1-4, 20×16 cm^2 in T5-6 and 80×100 cm^2 in T7-10. The particle flux at T1 is the highest, with 9.6 s spills of 10^{13} PoTs, it reaches 20MHz/mm^2 at the center of the tracking plane. In the muon spectrometer, the flux is significantly lower with a peak flux of 0.6MHz/mm^2. Time resolutions of ~40 ps for the beam spectrometer tracking planes and ~100 ps for the muon spectrometer ones should allow for the track and decay reconstructions. The list of all trackers specifications is reported in Table 2.

The 4D (particles position and time) tracking approach has been successfully pioneered by the NA62 collaboration, which has developed 3×6 cm^2 silicon pixel detectors with a pitch of 300 μm and a time resolution of 130 ps [11]. These detectors are capable of operating at a peak flux of 2 MHz/mm^2, being fully adequate for the muon spectrometer tracking planes. This technology can be also used in a hybrid approach, where silicon is used for the most illuminated region while more scalable technologies – such as MM, straw tubes, or scintillating fibers – are employed for the outer regions.

To match the flux at the beam spectrometer new silicon technologies are instead required. In the context of the LHC experiment upgrades for the High Luminosity phase – particularly the second upgrade of the LHCb Vertex Locator (VELO) – R&D programs for high-intensity 4D trackers were initiated and later joined by the NuTag collaboration. Such pixel detectors consist of a silicon sensor hybridized with readout electronics made of application specific integrated circuits (ASICs). These devices must be extremely thin to match the total material budget, allowing for less than 500 μm of silicon per tracking plane. Thermal management became so particularly challenging. The readout ASIC dissipates 1 W/cm^2 to 3 W/cm^2, and its power ultimately determines the time resolution. The only available technological solution by now is the micro-channel cooling plates, such as those developed for the NA62 GigaTracker and the LHCb VELO. These devices consist of a silicon plate a few hundred microns thick, encapsulating micro-channels through which a refrigerant circulates. Technological solutions on pixel sensors and integrated electronics have been developed and are still under study by the INFN TimeSPOT (2018–2021 and follow-ups) and IGNITE (2023, ongoing) projects. TimeSPOT has developed 3D silicon sensors, based on the so-called trench geometry (see Fig. 5).

Details on experimental methodologies and results can be found in [12]. 3D-trench sensors demonstrated outstanding performance both in time resolution and radiation resistance. They are capable of an intrinsic time resolution below 10 ps and withstand a fluence of at least 10^{17} n_{eq}/cm^2, without significant loss in timing and efficiency performance. TimeSPOT initiative started also to develop integrated

Table 2
Tracker specifications of the beam and muon spectrometers compared to the present NA62 Gigatracker and the future upgraded LHCb VELO. Simulations of the neutrino tagging presented in this document assume a material budget of 0.5% of a radiation length and a spill duration of 9.6 s.

Specifications [units]	Beam Spectro.	Muon Spectro.	LHCb-VELO(2028)	NA62-GTK (since 2014)
Peak dose [Mrad]	700	60	$>10^3$	16
Peak fluence [1MeVn$_{eq}$/cm^2]	1×10^{16}	6×10^{14}	5×10^{16}	4.5×10^{14}
Peak rate [MHz/mm^2]	20	0.6	10–100	2
Time resolution [ps]	<40	<100	<50	<130
Pixel pitch [μm]	300	300	45	300
Material budget [X$_0$]	<1%	<1%	0.8%	0.5%

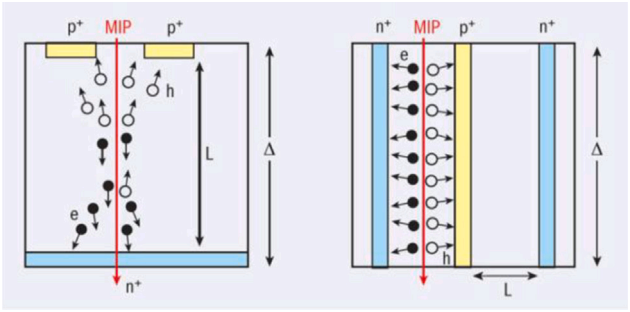


Fig. 5. Schematic representation of a 3D silicon sensor with trench geometry (right), compared with a standard planar one (left).

electronics with pixel readout in CMOS 28 nm technology, that is presently the only validated one [13] against the high dose expected in a neutrino tagging apparatus (above 1 Grad). The TimeSPOT starting developments are being finalized by the IGNITE project. IGNITE is developing an ASIC to read out a 256 × 256 pixel matrix, with a 45 μm pitch. The IGNITE ASIC integrates one fast amplifier and one TDC per pixel. Pre-processing capabilities and large bandwidth data readout facilities (100 Gbps) are also integrated. The ASIC is being designed mainly following the LHCb VELO Upgrade2 specifications, which are summarized in Table 2 together with the one, close but not identical, of the neutrino tagging. A parallel development named LA-Picopix is presently ongoing at CERN. Both the IGNITE and the LAPicopix developments aim to deliver their ASICs in 2026. High-Intensity 4D-Tracking techniques, satisfying the requirement given in Table 2, are technically extremely demanding. For this reason, having two parallel developments that face such a challenge with alternative approaches is an advantage.

6. Neutrino detectors

To maximize nuSCOPE potential, the facility requires detectors with great spacial and temporal resolution, that can exploit the unprecedented precision of the beam. In order to provide cross-section measurements in the same target materials as the ones of the next-generation long-baseline experiments, the two primary detectors will therefore utilize argon and water targets. The detailed detector choice will depend on the site implementation of nuSCOPE, but the total (fiducial) detector mass needs to be in the 500–1000 ton range.

6.1. Liquid-argon detector

The leading candidates for the argon-based detectors [14] at nuSCOPE are inspired by the ProtoDUNEs [15] and their future upgrades. Compared to the current ProtoDUNEs, all proposed upgrades preserve the imaging and particle reconstruction capabilities of DUNE at the GeV scale, while enhancing the performance of the photon detection system, to improve the energy resolution at the few-MeV scale. The capability to tag neutrinos beyond monitoring requires a time resolution better than 1 ns in the neutrino detectors and the time resolution in LAr TPC critically depends on the number of detected photoelectrons; so, enhancing the photon detection system becomes essential to enable neutrino tagging. The ideal detector for nuSCOPE would be one of the current ProtoDUNEs equipped with an upgraded timing system. Also the implementation of a dedicated cosmic ray veto system could be very valuable, given the slow proton extraction of nuSCOPE.

6.2. Water-based detector

Water is the target material for Hyper-Kamiokande [16]. Water Cherenkov (WC) technology offers an ideal setting for nuSCOPE operations, even in tagged mode, as it can achieve sub nanosecond time resolution at large scales with limited light coverage, due to the inherently faster emission of Cherenkov light compared to liquid argon scintillation light. However, it poses problem about events containment and precise reconstruction of neutrino interactions and energy; a dedicated detector with a fiducial volume of a few hundred tons would be required. Further enhancement of WC particle identification capability could be achieved by replacing the water target with modern water-based scintillators. This novel technology, pursued by several experimental groups, aims to overcome the limitations of Water Cherenkov detectors in medium- and large-scale experiments.

6.3. Reference detector parameters

The studies presented here are based on a reference liquid argon (LAr) detector with a 500-ton fiducial mass, positioned 25 m from the end of the decay tunnel. The front face measures 4×4 m^2, with a total length of 22.3 m. The LAr TPC is assumed to have a time resolution improved to 300 ps compared to the current ProtoDUNE, thanks to an enhanced photon detection system as planned for DUNE Phase II upgrades [17]. We are optimizing also the design of a water-based detector and are carrying out similar studies using this type of detector.

7. Flux characterization and a priori measurements of neutrino energy

7.1. Flux constraints

In conventional neutrino beams, the knowledge of the neutrino flux at the detector is limited to a 5%–10% level [18,19]. The dominant systematic is given by the uncertainties in the yield of mesons produced in the interaction of the primary proton beam with the target, known as the hadroproduction systematics. This limitation is overcome by the monitoring technique, where the charged leptons produced together with the neutrinos in the meson decays are measured directly in the instrumented decay tunnel and directly correlated with the neutrino flux at the detector. The need to rely on simulations of the hadronic components in beam production is further eliminated by beam tagging method. It provides a direct measurement of the input neutrino flux, by measuring each mesonic decay of the beam and associating each observed neutrino interaction with its parent in time and space. The performance of the time coincidence is dominated by the time resolution of the LAr detector (300 ps, see Section 6.3), i.e. much worse than

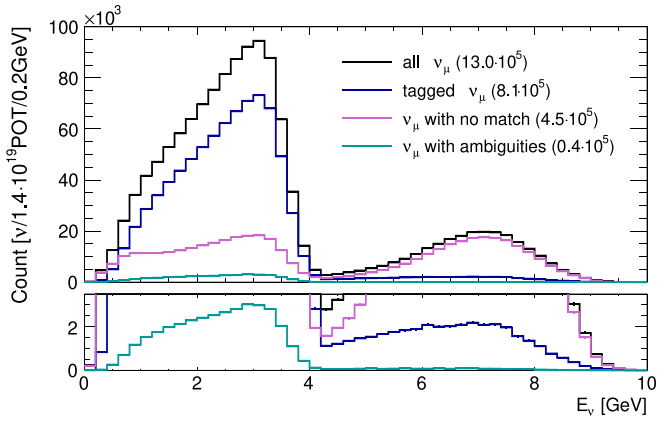


Fig. 6. ν_μ interaction rates as a function of energy. The interaction sample (black) is divided into three categories: tagged neutrino interactions, i.e., matched to a single decay (dark-blue); interactions matched to no-decay (pink); interactions matched to multiple decays (light-blue). The numbers in the legend indicate the total number of interactions in each category.

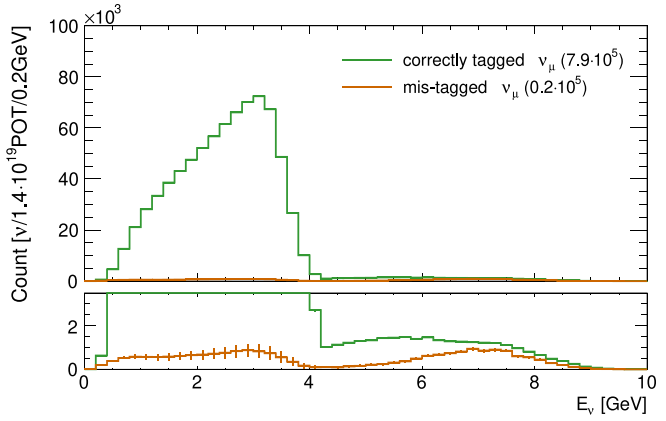


Fig. 7. ν_μ interaction rates as a function of energy. The tagged sample is subdivided into two sub-samples: interactions associated with the correct meson decay (green); interactions associated with a wrong meson decay (orange). The numbers in the legend indicate the total number of interactions in each category.

the tagging trackers time resolution (see Section 5). The performance of the space coincidence is dominated by multiple scattering in the tagging trackers. For the 0.5% radiation length tracker planes, the precision is O(1) mrad, corresponding to ∼40 mm in the LAr detector, i.e. much worse than the LAr spatial resolution.

The association of a given neutrino interaction with a measured meson decay can result in three possible outcomes: no match is found (no match case); multiple matches are found (ambiguous case); a single match is found (tagged case). In the tagged case, the associated decay can either be the correct one (correctly tagged case) or a pile-up decay (mistag case).

Figs. 6 and 7 show the distributions of these categories. It can be noted that for neutrinos with energies below 4 GeV (i.e., mostly from pion decays), most of the observed neutrino interactions are associated with their correct parent meson decay, with wrong and ambiguous matches remaining at a level of a few %. These performances significantly degrade for neutrinos with energies above 4 GeV (i.e. mostly from kaon decays) due to the reduced acceptance of the spectrometer for large-angle muons produced in kaon decays.

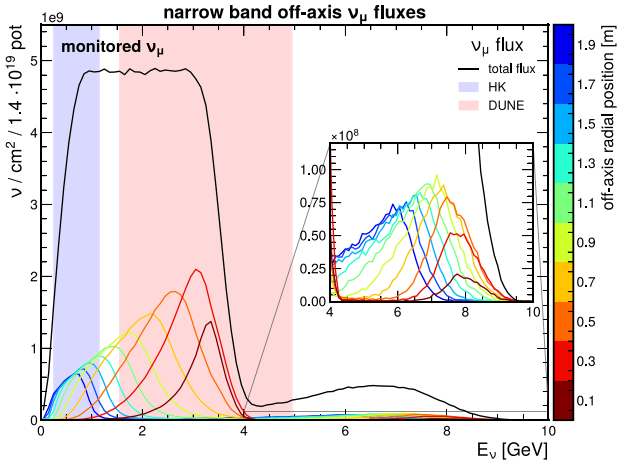


Fig. 8. ν_μ narrow band off-axis fluxes at different radial distances on the detector surface. The black line shows the total flux, considering the total squared surface of the exposed detector face, and the colored lines show the fluxes incident on filled discs of 20 cm at different radial positions on the detector surface. The radial position is given by the color scale alongside each plot. Only monitored neutrinos are shown, i.e. neutrinos produced from decays occurring along the instrumented decay tunnel. The inlay shows a zoom on the contribution of neutrinos from kaon parents in the 4–10 GeV energy range.

7.2. Narrow-Band Off-Axis technique

The energy of ν_μ produced in $\pi^+ \to \mu^+\nu_\mu$ and $K^+ \to \mu^+\nu_\mu$ decays is correlated to the emission angle, due to the two-body decay kinematics. The detector is exposed to a range of incoming neutrino directions, due to proximity to the neutrino beam and its large size. As a result, neutrinos interacting at different off-axis angles span different energy ranges. The off-axis technique has already been exploited by a cross-section measurement from the T2K experiment [20], and is central for the PRISM technique [21].

In the nuSCOPE narrow-band beam we have a parent meson momentum knowledge at O(10%) and this enables an a priori determination of the neutrino energy without relying on the reconstruction of final-state particles. This is the fundamental principle of the Narrow-Band Off-Axis (NBOA) technique, which can be applied to ν_μ fluxes from $\pi_{\mu\nu}$ and $K_{\mu\nu}$ decays. Neutrinos interacting at different off-axis angles are identified by defining a set of cylinders within the detector volume, corresponding to different radii where interaction vertices occur. The radial distances covered by the detector surface correspond to an angular range of 0–4.5°, and, by selecting specific radial slices, a neutrino flux narrower than the total flux can be probed. We define 10 radial slices, each spanning a 20 cm window; the contribution of the total ν_μ flux within each radial slice is shown in Fig. 8.

The flux exhibits the characteristic dichromatic energy spectrum of a narrow-band beam, with a low-energy component (1–4 GeV) from $\pi_{\mu\nu}$ and a high-energy component (5–8 GeV) from $K_{\mu\nu}$. As expected, the neutrino energy decreases with increasing radial distances for both components.

7.3. Neutrino energy from tagging

Beam tagging allows to measure the energy of each tagged neutrino interaction from the kinematics of the associated parent meson decay ($E_\nu = E_{K,\pi} - E_\mu$), independently of the neutrino detector response. The energy resolution is dominated by multiple scattering in the beam and muon spectrometers tracking planes. Fig. 9 shows the expected resolution for tracker planes of 0.5% and 1% radiation length. The neutrino energy resolution lies in the sub-% range, below 0.4% for E_ν > 1 GeV.

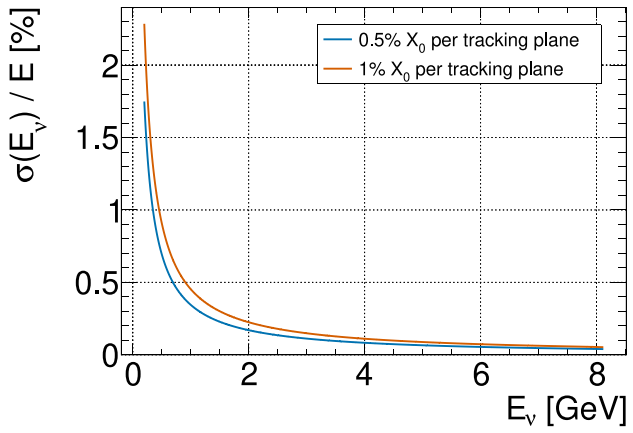


Fig. 9. Expected energy resolution of tagged neutrino interactions from π and K decays, as a function of the true neutrino energy for a material budget per tracking plane of 0.5% (blue) and 1% (orange) of a radiation length.

Table 3
ν_μ and ν_e event rate integral.

Channel	Events/1.4 × 10^{19} PoT
Total ν_μ	1.3 × 10^6
Total ν_e	1.7 × 10^4
Total monitored ν_μ	1.0 × 10^6
Total monitored ν_e	1.2 × 10^4
Total tagged ν_μ	7.6 × 10^5

8. Neutrino cross-section measurements

nuSCOPE can perform a lot of cross section measurements, using the monitored neutrino beam and the NBOA technique. It provides also the unique opportunity to perform measurements using tagged neutrinos. This provides prospects for performing measurements where the neutrino energy is known on an event-by-event basis. As an example we show the measurement of flux averaged ν_μ CC cross-sections, first using the NBOA and then the tagged technique.

We assume the use of the argon-based reference detector described in Section 6.3. Simulated data correspond to a 5 years of SPS neutrino run mode with 8.5 GeV/c momentum secondaries. The total CC event rates are summarized in Table 3.

8.1. Flux-averaged ν_μ CC-inclusive cross-section with NBOA technique

Since the visible event rate for a neutrino experiment results from the convolution of the neutrino flux and the interaction cross-section, it is only possible to measure the total cross-section for a process averaged over the range of available energies. The flux-averaged cross-section $\langle\sigma\rangle_\Phi$ (in cm^2/nucleon) is defined as

$$\langle\sigma\rangle_\Phi = \frac{N_{events}}{\Phi N_{target} N_{PoT}} \quad (1)$$

where N_{events} is the number of expected events in the detector (as predicted by simulation), Φ is the neutrino flux integral (expressed in ν/cm^2/PoT), N_{target} is the number of nucleons in the considered volume and N_{PoT} is the total exposure in protons on target, i.e. 1.4 × 10^{19} PoT. This technique is equivalent to counting the number of neutrino interactions that have a charged lepton consistent with a muon in the final state, regardless of other products. For wide-band beams, the measurement of the ν_μ CC inclusive cross-section is intrinsically limited by the range spanned by the neutrino flux, since the neutrino energy is not known on an event-by-event basis.

Since the $\pi_{\mu\nu}$-like and the $K_{\mu\nu}$-like contributions to the neutrino flux are well separated at ∼4 GeV in true neutrino energy (See Fig. 8), applying energy cut, we extract two flux-averaged cross-sections for each NBOA flux, one for $\pi_{\mu\nu}$ decays and one for $K_{\mu\nu}$ decays. The resulting flux-averaged cross-sections, along with statistical uncertainties, are shown in Fig. 10.

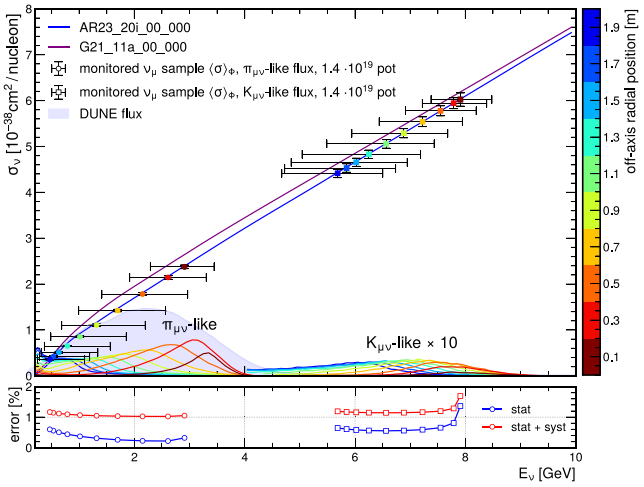


Fig. 10. Flux averaged ν_μ CC inclusive cross-section as a function of neutrino energy using the NBOA technique. The colored lines correspond to the NBOA fluxes at different radial distances, given by the colored scale to the right of the figure. The $K_{\mu\nu}$ component of each flux has been artificially inflated by a factor of 10 for illustration purposes. Each NBOA flux has a corresponding predicted measurement point of the same color. Horizontal error bars encase the 68% percentiles with respect to the mean energy for the NBOA fluxes. The underlying figure shows the size of uncertainties due to available statistics (blue) and considering also systematic uncertainties related to the monitored flux prediction, assumed to be ∼1%, (red). The measurements are compared to the AR23 20i 00 000 model (blue) and the G21 11a 00 000 model (purple). The DUNE near detector flux is shown for reference using an arbitrary normalization.

Thanks to the large size of the detector assumed in this setup, the statistical errors associated with such a measurement are almost always below 1%. The measurement would therefore be entirely limited by systematic uncertainties, that are anyway kept at the 1% level thanks to the monitoring of charged leptons.

8.2. ν_μ CC-inclusive cross-section with the tagged neutrino sample

The total ν_μ CC inclusive cross-section can also be measured with tagged neutrinos.

Despite the reduction in statistics because tagged neutrinos can only be found in the decay tunnel, and taking into account the tagging efficiency, the total event rate is still significant and comparable to that obtained using the NBOA technique (see Table 3). The $K_{\mu\nu}$ contribution is smaller than in the NBOA case due to the lower tagging efficiency in this region, due to the larger angle of muons from kaons that fall outside the geometrical acceptance of the muon spectrometer. The $\pi_{\mu\nu}$ contribution is similar to the one obtained with the monitored beam.

The unprecedented determination of the neutrino energy on an event-by-event basis made possible by the tagged beam allows us to perform the measurement directly as a function of the neutrino energy, instead of extracting a flux-averaged cross-section for each off-axis position. The projected measurement is shown in Fig. 11.

The total statistics at each neutrino energy allow us to extract a cross-section with associated statistical uncertainties of less than 5% across the entire considered energy range. The statistical error on the measurement is below ∼1% between 1–4 GeV, corresponding to the higher statistics coming from $\pi_{\mu\nu}$ decays. The small increase in statistical error around 4.5 GeV is due to the transition region between the $\pi_{\mu\nu}$ and $K_{\mu\nu}$ populations, and the statistical error stays at the level

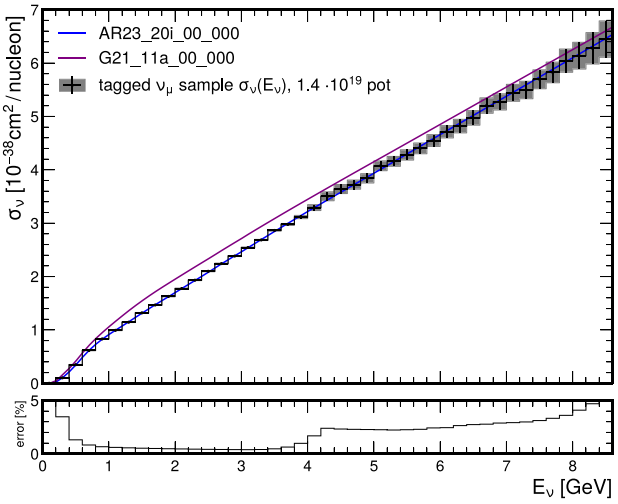


Fig. 11. Projected measurement of the ν_μ CC inclusive integrated cross-section as a function of neutrino energy using tagged neutrinos. The reference model (AR23 20i 00 000, in blue) is compared to the alternative model G21 11a 00 000, shown in purple. The error bars represent the statistical error expected on the measurement, also shown below the main figure.

of 2%–3% for the $K_{\mu\nu}$ region. It is important to note that thanks to the tagging, this measurement has negligible flux systematic uncertainties.

9. Conclusions

nuSCOPE addresses a fundamental limitation in neutrino physics: the lack of precise knowledge of neutrino cross-sections at the GeV scale. This uncertainty currently hinders the physics potential of long-baseline experiments like DUNE and Hyper-Kamiokande. nuSCOPE is based on two innovative techniques, whose proof-of-principle has been demonstrated in recent years by the NP06/ENUBET and NuTag Collaborations. nuSCOPE introduces a novel beam that monitors leptons at the single-particle level and can tag both the parent meson and the accompanying muon of the neutrinos interacting in the detector. The proposed beamline leverages the CERN-SPS to produce a highly controlled neutrino beam. The proposal integrates liquid argon and water Cherenkov detectors, ensuring high-resolution event reconstruction. The instrumented decay tunnel provides real-time flux monitoring using tracking detectors and calorimeters to measure lepton production. The ability to measure neutrino energy on an event-by-event basis represents a groundbreaking improvement over conventional techniques. With a percent level of accuracy in energy and flux normalization, neutrino-nucleus cross-section measurements could reach precision levels comparable to electron-nucleus cross-sections, reducing systematic errors in oscillation experiments. While the current focus has been put on neutrino cross-sections, additional studies are being performed to address the potential of nuSCOPE in terms of BSM physics topics that could benefit from the presence of a high granularity massive detector close to a proton and hadron beam dump associated with an unprecedented control over neutrino-originating decays. The nuSCOPE project has the potential to revolutionize neutrino cross-section measurements, supporting the next generation of neutrino physics experiments.

Declaration of competing interest

The authors declare that they have no known competing financial interests or personal relationships that could have appeared to influence the work reported in this paper.

Acknowledgments

This project is supported by the Agence Nationale de la Recherche (ANR,France) through the PIMENT project (ANR-21-CE31-0027) and the MRSINT project (ANR-25-MRS1-0024), by the Italian Ministry of University and Research through the GIGANU project (PRIN 2022BZ 2ABA), by the Ministry of Science Education and Youth of Republic of Croatia Grant No. PK.1.1.10.0002, and by Swiss National Science Foundation (SNSF) and Croatian Science Foundation (HRZZ) under grant MAPS IZ11Z0_230193.

References

[1] L. Alvarez-Ruso, et al., Prog. Part. Nucl. Phys. 100 (2018) 1, http://dx.doi.org/10.1016/j.ppnp.2018.01.006.
[2] T. Katori, M. Martini, J. Phys. G 45 (1) (2018) 013001, http://dx.doi.org/10.1088/1361-6471/aa8bf7.
[3] A. Longhin, L. Ludovici, F. Terranova, Eur. Phys. J. C 75 (2015) 155, http://dx.doi.org/10.1140/epjc/s10052-015-3378-9.
[4] F. Acerbi, et al., Eur. Phys. J. C 83 (10) (2023) 964, http://dx.doi.org/10.1140/epjc/s10052-023-12116-3.
[5] A. Baratto-Roldan, M. Perrin-Terrin, E.G. Parozzi, M.A. Jebramcik, N. Charitonidis, Eur. Phys. J. C 84 (10) (2024) 1024, http://dx.doi.org/10.1140/epjc/s10052-024-13324-1.
[6] F. Acerbi, et al., nuSCOPE - A short-baseline neutrino beam at CERN for high-precision cross-section measurements. arXiv:2503.21589v2.
[7] F. Acerbi, et al., NP06/ENUBET Annual Report 2022 for the SPSC, Tech. Rep., https://cds.cern.ch/record/2805716.
[8] F. Acerbi, et al., Construction, commissioning, and performance of the ENUBET demonstrator. arXiv:2608.02164.
[9] F. Acerbi, et al., J. Instrum. 15 (08) (2020) P08001, http://dx.doi.org/10.1088/1748-0221/15/08/P08001.
[10] A. Kallitsopoulou, et al., Nucl. Instrum. Methods A 1069 (2024) 169920, http://dx.doi.org/10.1016/j.nima.2024.169920.
[11] G. Aglieri-Rinella, et al., J. Instrum. 14 (2019) P07010, http://dx.doi.org/10.1088/1748-0221/14/07/P07010.
[12] F. Borgato, et al., Front. Phys. 12 (2024) 1393019, http://dx.doi.org/10.3389/fphy.2024.1393019.
[13] G.M. Termo, et al., Nucl. Instrum. Methods A 1065 (2024) 169497, http://dx.doi.org/10.1016/j.nima.2024.169497.
[14] W.M. Bonivento, F. Terranova, Rev. Mod. Phys. 96 (4) (2024) 045001, http://dx.doi.org/10.1103/RevModPhys.96.045001.
[15] A. Abed Abud, et al., J. Instrum. 17 (01) (2022) P01005, http://dx.doi.org/10.1088/1748-0221/17/01/P01005.
[16] K. Abe, et al., Hyper-Kamiokande design report. arXiv:1805.04163.
[17] A. Abed Abud, et al., J. Instrum. 19 (12) (2024) P12005, http://dx.doi.org/10.1088/1748-0221/19/12/P12005.
[18] K. Abe, et al., Phys. Rev. D 87 (1) (2013) 012001, http://dx.doi.org/10.1103/PhysRevD.87.012001, Addendum; Phys. Rev. D 87 (2013) 019902.
[19] L. Aliaga, et al., Phys. Rev. D 94 (9) (2016) 092005, http://dx.doi.org/10.1103/PhysRevD.94.092005, Addendum; Phys. Rev. D 95 (2017) 039903.
[20] K. Abe, et al., Phys. Rev. D 108 (11) (2023) 112009, http://dx.doi.org/10.1103/PhysRevD.108.112009.
[21] S. Bhadra, et al., Letter of intent to construct a nuPRISM detector in the J-PARC neutrino beamline. arXiv:1412.3086.